

Role of Co–W Interaction in the Selective Growth of Single-Walled Carbon Nanotubes from CO Disproportionation

José E. Herrera and Daniel E. Resasco*

School of Chemical Engineering and Materials Science, University of Oklahoma, Norman, Oklahoma 73019

Received: December 2, 2002; In Final Form: February 6, 2003

A combination of characterization techniques has been employed to obtain a full description of the structure and chemical state of a series of Co–W/SiO₂ catalysts used for the production of single-walled carbon nanotubes (SWNT) by CO disproportionation at 750–950 °C. The state of Co and W on a series of silica-supported catalysts has been investigated using extended X-ray absorption fine structure, X-ray absorption near-edge spectroscopy, ultraviolet–visible diffuse reflectance spectroscopy, H₂ temperature-programmed reduction, and Raman spectroscopy. The results are compared to those obtained in a previous study on a highly selective CoMo catalyst. Strong similarities and interesting differences between the two catalytic systems are revealed. First, it has been found that, similar to the Co–Mo system, the selectivity of the Co–W catalysts toward SWNT strongly depends on the stabilization of Co species in a nonmetallic state before exposure to CO. This stabilization is a consequence of the interaction of Co with tungsten oxide. From the detailed characterization conducted over the catalyst series it has been concluded that after calcination, W is in the form of a well-dispersed W(VI) oxide while Co is either interacting with W in a superficial Co tungstate like structure (at low Co:W ratios) or as a noninteracting Co₃O₄ phase (at high Co:W ratios). From the SWNT growth studies and the TPR data it is shown that a carefully chosen reduction pretreatment is critical for the good performance of the selective Co–W catalyst. The comparison of SWNT selectivity and TPR profiles between two selective Co–Mo and Co–W catalysts suggests that both activity and selectivity toward SWNT production strongly depend on the degree of the interaction between Co and W (or Co and Mo) and a specific partial reduction pretreatment.

1. Introduction

Single-wall carbon nanotubes (SWNT) can be considered as one of the building blocks for nanoscale science and nanotechnology. They exhibit exceptional chemical and physical properties that have opened a vast number of potential applications.¹ Among the various alternatives investigated in the past few years for production of SWNT, the catalytic decomposition of carbon-containing molecules appears as a promising technique because it has the potential to be scaled up at a relatively low cost. A number of researchers have investigated different catalyst formulations and operating conditions.^{2–4} Yet, obtaining high-quality SWNT has not been always possible with this method. Our group has focused on the disproportionation of CO on several bimetallic catalysts, which exhibited a high selectivity toward the production of SWNT at relatively low temperatures. Among the various formulations investigated, we previously reported that Co–Mo catalysts supported on silica gel and having low Co:Mo ratios exhibited the best performance.^{5,6} We have explained this performance on the basis of a Co–Mo interaction that becomes optimal when the support is SiO₂ because other supports such as alumina or MgO induce segregation of Co from Mo and therefore a limited Co–Mo interaction.

The Co–Mo system is a catalyst commonly employed in petroleum refining for hydrotreating processes. However, most studies on these catalysts have focused on alumina-supported

systems because alumina interacts with the metals with the appropriate strength to generate the species with the optimum hydrotreating activity in the sulfided state. Due to the strong chemical similarities with Mo, tungsten has been investigated as a catalyst component. For example, it has been found that the addition of W to the Co–Mo bimetallic catalyst significantly increases the hydrotreating activity.⁷ However, a Co-promoted W catalyst without Mo is generally regarded as an unsuccessful combination for hydrotreating. Reports of supported Co–W catalysts are limited and the reason for the lack of synergy between Co and W in the sulfide state is still unclear.^{8,9}

In the present contribution we have turned our attention to the Co–W catalytic system for SWNT production and have designed a characterization strategy on the basis of the abundant precedent literature and our own work on the application of these techniques to investigate this bimetallic system.⁶ We have been able to put together a detailed picture of the structure of this catalyst, and built up an analogy with the Co–Mo system, which can be used to explain the variations in selectivity toward SWNT observed when the catalyst formulations, pretreatment, and/or reaction conditions are changed.

2. Experimental Section

2.1. Catalysts Preparation and Pretreatment. A series of mono- and bimetallic Co–W catalysts supported on silica was prepared by incipient wetness impregnation. The bimetallic samples, prepared by coimpregnation of aqueous ammonium metatungstate and Co nitrate solutions, had Co:W molar ratios of 2:1, 1:1, 2:3, 3:4, 1:2, and 1:3. In this series, the amount of

* To whom correspondence should be sent. Address: 100 East Boyd St. Phone: (405) 325-4370. Fax: (405) 325-5813. E-mail: resasco@ou.edu.

Co was kept constant for all catalysts at 1.3 wt %, while the amount of W was varied accordingly. Three monometallic catalysts were prepared with loadings of 0.02 wt % Co, 1.3 wt % Co, and 4.6 wt % W, respectively. The SiO₂ support obtained from Aldrich had an average pore size of 6 nm, BET area 480 m²/g, pore volume 0.75 cm³/g, and particle sizes in the range 70–230 mesh. Five grams of SiO₂ support was impregnated using a liquid-to-solid ratio of 0.6 cm³/g. After impregnation, the solids were dried overnight at 120 °C and then calcined in a horizontal fixed bed reactor for 3 h at 500 °C in dry-air flow of 50 scc/min.

2.2. Catalyst Characterization. The UV/vis spectra of the calcined catalysts were recorded using a Shimadzu double beam spectrometer UV-2101 with an integrating sphere for diffuse reflectance. Barium sulfate was used as the reflectance standard. Several W and Co compounds, including WO₃, Na₂WO₄·2H₂O, (NH₄)₁₀W₁₂O₄₁·5H₂O, CoWO₄, and CoMoO₄ were used as references. Before each analysis, the samples were dried in air at 120 °C.

The X-ray absorption data were obtained at the National Synchrotron Light Source at Brookhaven National Laboratory, using beam line X-18B equipped with a Si(111) crystal monochromator. The X-ray ring at the NSLS has an energy of 2.5 GeV and ring current of 80–220 mA. The EXAFS experiments were conducted in a stainless steel sample cell at liquid nitrogen temperature. Six scans were recorded for each sample. The average spectrum was obtained by adding the six scans. The pre-edge background was subtracted by using power series curves. Subsequently, the post-edge background was removed using a cubic spline routine. The spectra were normalized by dividing by the height of the absorption edge. The spectra of Co₃O₄ and CoWO₄ were also obtained at liquid nitrogen temperature and used as references.

The temperature programmed reduction (TPR) experiments were conducted by passing a continuous flow of 5% H₂/Ar over approximately 30 mg of the calcined catalyst at a flow rate of 10 cm³/min, while linearly increasing the temperature at a heating rate of 8 °C/min. The hydrogen uptake as a function of temperature was monitored using a thermal conductivity detector, SRI model 110 TCD. The TCD was calibrated for hydrogen consumption using TPR profiles of known amounts of CuO and relating the peak area to hydrogen uptake.

The Raman spectra of both fresh catalysts and nanotubes were obtained in a Jovin Yvon-Horiba LabRam 800 equipped with a CCD detector and with three different laser excitation sources having wavelengths of 632 (He–Ne laser), 514, and 488 nm (Ar laser). Typical laser powers ranged from 3.0 to 5.0 mW; integration times were around 15 s for each spectrum; ten Raman spectra were averaged for each sample.

2.3. Production and Characterization of Carbon Nanotubes. To study the effect of reaction parameters in the Co–W system, the production of SWNT by CO disproportionation was conducted on a catalyst with a Co:W molar ratio of 1:3 under different conditions. The choice of this particular composition was based on previous studies in which we found that the silica-supported Co–Mo system displays a very high selectivity in the production of single wall nanotubes by CO disproportionation only when low Co:Mo molar ratios were used.¹⁰ By contrast, when high Co:Mo ratios were used, undesired forms of carbon, such as graphite and irregular nanofibers were obtained. For the SWNT production on the Co–W/SiO₂ catalysts, 0.5 g of a calcined sample was placed in a horizontal tubular packed-bed reactor; the reactor was 12 in. long and had a diameter of 0.5 in.. After loading the catalyst, the reactor was

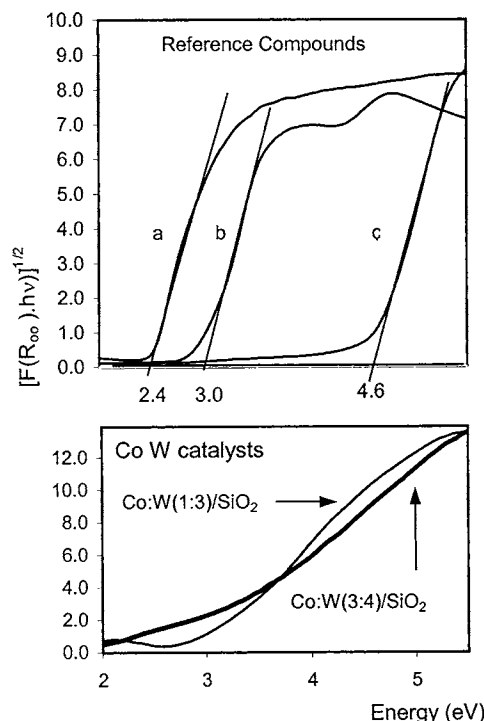


Figure 1. Lower panel: UV absorption spectra for two Co:W/SiO₂ calcined catalysts; heavy line: Co:W(3:4), light line Co:W(1:3). Upper panel: (a) WO₃, (b) (NH₄)₁₀W₁₂O₄₁·5H₂O, and (c) Na₂WO₄·2H₂O references. The value of the energy gap for these last three species is also indicated.

heated in 50 scc/min H₂ flow to different temperatures in the range 500–1000 °C at 10 °C/min; once the desired reduction temperature was reached, the system was heated under 50 scc/min flow of He at the same rate to the specified reaction temperature, which ranged from 750 to 950 °C. Subsequently, CO was introduced at a flow rate of 850 cm³/min at 84 psia for 2 h. At the end of each run, the system was cooled under He flow. The total amount of deposited carbon was determined by temperature-programmed oxidation (TPO) following the method described elsewhere.⁵

3. Results

3.1. Characterization of the Catalysts. *3.1.1. Diffuse Reflectance UV/Visible Spectroscopy (UV/V-DRS).* We have used UV/V-DRS to study the state of both W and Co in the oxidic form, after calcination in air at 500 °C. To estimate the band energy gap of d⁰ oxides, it has been recommended to use the square root of the Kubelka–Munk function multiplied by the photon energy, and plot this new function versus the photon energy.¹¹ The position of the absorption edge can then be determined by extrapolating the linear part of the rising curve to zero. The values thus obtained carry information about the average domain size of the oxide nanoparticles. It has been shown that the energy band gap decreases as the domain size increases.^{11,12} Therefore, a comparison can be made between the energy of the samples under investigation and those of references of known domain size. This comparison is made in Figure 1, which shows the absorption edges of several WO_x species together with those of two different Co:W/SiO₂ catalysts. As expected, the band gap energies in the reference series decrease as the domain size increases. Those for the two Co:W/SiO₂ catalysts investigated lie between the values corresponding to (NH₄)₁₀W₁₂O₄₁·5H₂O and WO₃. From this comparison it can be inferred that the W species in the calcined

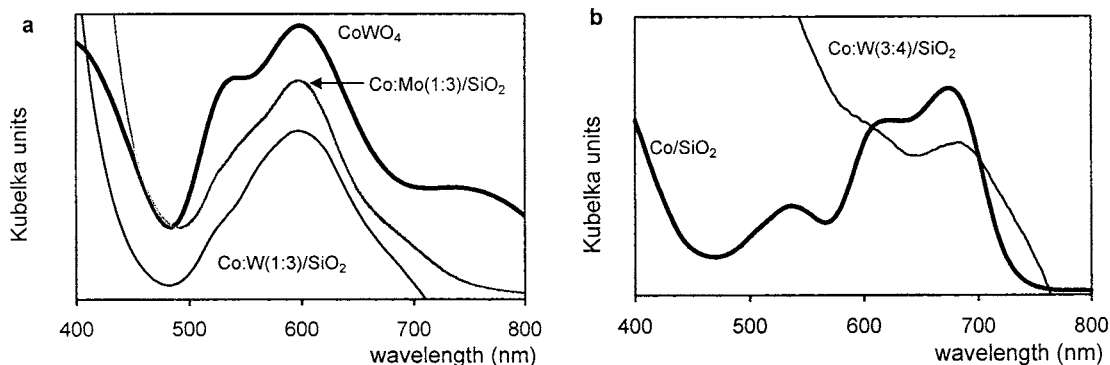


Figure 2. Visible spectra for two calcined bimetallic Co:W/SiO₂ catalysts with different Co:W ratios (1:3 and 3:4) and that for a monometallic Co/SiO₂. The spectra of a bimetallic CoMo(1:3)/SiO₂ catalyst and CoWO₄ (adapted from ref 13) are included for comparison.

catalysts have relatively small domain sizes and that little difference is observed in the state of W as the Co:W ratio changes. The presence of a small contribution of WO₃ species is clear on the CoW(3:4)/SiO₂ sample because a small tail can be observed below 3.0 eV; nevertheless, most of the W is certainly in a high state of dispersion.

In addition to the charge-transfer bands due to W, appearing in the UV region, the visible spectra of the bimetallic catalysts present bands in the 500–750 nm region, which did not appear for the W/SiO₂ catalyst. These bands are associated with Co species and are ascribed to d–d transitions (${}^4T_{2g} \rightarrow {}^4A_{2g}$ and ${}^4T_{2g} \rightarrow {}^4T_{1g}(P)$) of high-spin octahedral Co complexes.^{6,13,14} Figure 2 shows the DRS spectra in this region for three calcined catalysts, Co:W(3:4)/SiO₂, Co:W(1:3)/SiO₂, and Co/SiO₂. The spectrum for the Co:W(1:3) catalyst is very similar to that of CoWO₄, in which Co is in an octahedral environment. For comparison, Figure 2a includes the spectrum of a CoMo(1:3)/SiO₂ catalyst, which as shown previously, is highly selective for the production of SWNT and has all the Co in an octahedral environment. The small difference in the position of the maximum in the spectrum of the Co–W catalysts compared to that of the Co–Mo catalyst observed in Figure 2a is attributed to a difference in the strength of the ligand field. Nevertheless, the identical shape of the spectra of both samples indicates that both catalysts have the same ligand symmetry around Co. By contrast, the shape of the spectrum of the Co:W(3:4)/SiO₂ catalyst shown in Figure 2b, was markedly different and exhibited the appearance of a band at around 680 nm. This band was in turn the dominant feature in the pure Co catalyst and can be associated with Co₃O₄ species, which as shown below, are present in the pure Co catalyst in the calcined state. Therefore, it can be concluded that, similarly to the Co–Mo catalytic system, a catalysts with low Co:W ratio exhibits most of the Co in interaction with W but, as the Co:W ratio increases, free Co oxide starts appearing.

3.1.2. X-ray Absorption Spectroscopy (EXAFS/XANES). Figure 3 compares the Co K-edge ($E_0 = 7709$ eV) XANES spectra for two bimetallic Co:W(1:3)/SiO₂ and Co:Mo(1:3)/SiO₂ catalysts in the calcined form together with those of two reference compounds, CoWO₄ and CoMoO₄. Except for some small differences in the intensity of the first peak in the edge, the four spectra look remarkably similar. In agreement with the conclusions reached from the UV/vis results, the X-ray absorption data indicate that in a catalyst with low Co:W (or Mo) molar ratio, Co is interacting strongly with W (or Mo) in a local environment similar to that in CoWO₄ or CoMoO₄. By contrast, the Co edges from the Co:W(2:1) and CoMo(2:1) catalysts, which contain excess Co, are very different from that of the cobalt tungstate (molybdate) reference. As shown in Figure 4,

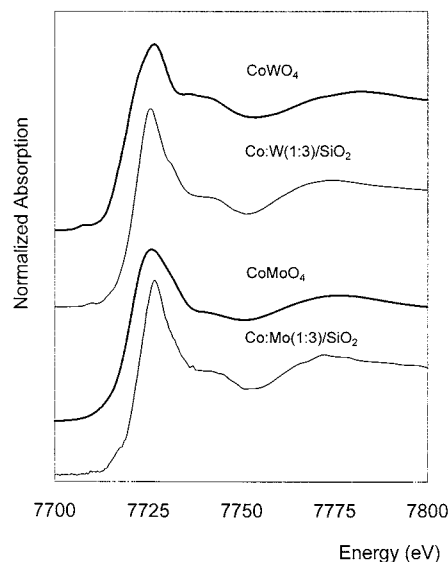


Figure 3. Co K edge (7709 eV) XANES spectra of calcined CoW(1:3)/SiO₂ and Co:Mo(1:3)/SiO₂ catalysts compared to CoWO₄ and CoMoO₄ used as a references.

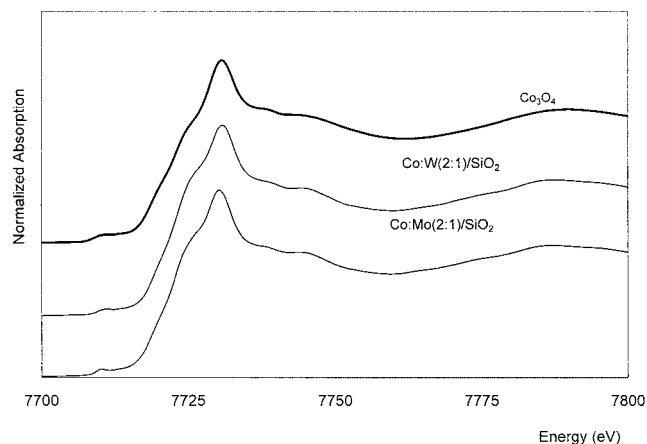


Figure 4. Co K edge XANES spectra of a calcined CoW(2:1)/SiO₂ and Co:Mo(2:1)/SiO₂ catalysts and for a Co₃O₄ analytical sample.

the XANES of these catalysts are in fact very similar to that of Co₃O₄.

The EXAFS data were in good agreement with the conclusions reached from the XANES analysis. As shown, in Figure 5, the Fourier transform for the calcined catalyst becomes very similar to that of Co₃O₄ as the Co:W ratio increases, indicating that this oxide is the predominant form present at high Co:W ratios. On the other hand, the results on the sample with low

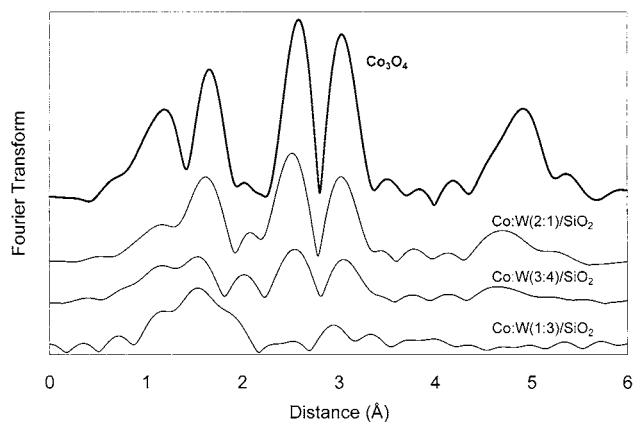


Figure 5. Fourier transforms of the k^3 EXAFS data of the Co K edge obtained on the calcined CoW(1:3)/SiO₂, CoW(3:4)/SiO₂, and CoW(2:1)/SiO₂ catalysts and for Co₃O₄ reference.

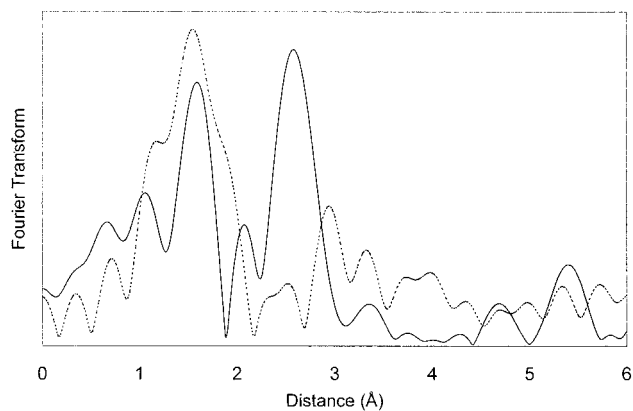


Figure 6. Fourier transforms of the k^3 EXAFS data of the Co K edge, obtained on the calcined Co:W(1:3)/SiO₂ catalyst (dotted line) and on a CoWO₄ reference (solid line).

Co:W ratio require some further consideration. While most of the Co in this catalyst is forming a CoWO₄-like phase, only a fraction of W participates in this compound. The rest of the W is in a dispersed tungsten oxide form, as demonstrated by the results obtained by UV/vis spectroscopy. We propose that, similar to the Co–Mo system, the Co is in a CoWO₄-like phase on the basis of the XANES data, which suggest that the local environment of Co in the Co:W(1:3) catalyst is very similar to that in CoWO₄. At the same time, the EXAFS data are significantly different from that of the bulk CoWO₄ compound. This comparison is made in Figure 6, which shows the Fourier transforms for the K-edge of Co in the calcined Co:W(1:3)/SiO₂ catalyst, together with that of bulk CoWO₄. The low intensity observed in the catalyst for the peak between 2.0 and 3.0 Å, clearly observable for the cobalt tungstate, shows that bulk CoWO₄ is not present, but rather a highly dispersed CoWO₄-like structure, coexisting with well-dispersed W oxide species.

3.1.3. Temperature Programmed Reduction (TPR). The reduction profiles of calcined monometallic Co/SiO₂, Mo/SiO₂, and W/SiO₂ catalysts together with that of the bimetallic Co:Mo(1:3)/SiO₂ and Co:W(1:3)/SiO₂ catalysts are shown in Figure 7. The TPR profile of the Co monometallic catalyst shows two peaks at 360 and 445 °C, which can be ascribed to the reduction of Co oxide species. The reductions of the monometallic W and Mo catalysts also exhibit two peaks, but they appear at much higher temperatures than those of Co; moreover it is evident that the reduction of the W/SiO₂ catalyst starts at higher temperatures than that of the Mo/SiO₂ catalyst.

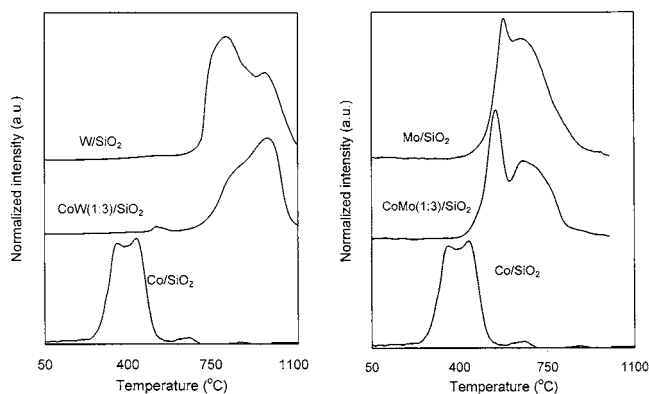


Figure 7. TPR profiles of several mono- and bimetallic cobalt/tungsten and cobalt/molybdenum catalysts. The TPR was conducted with 5% H₂/Ar at a heating rate of 8 °C/min.

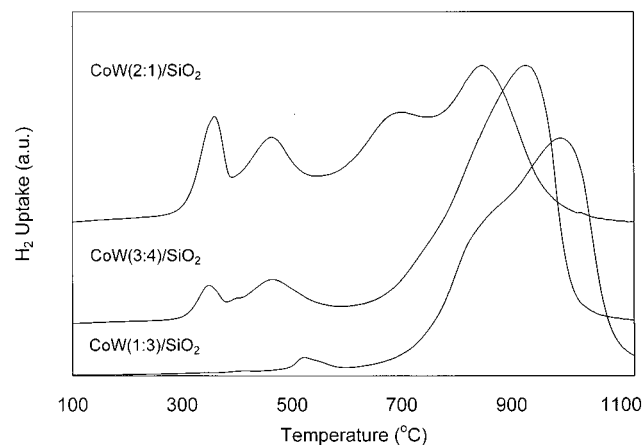
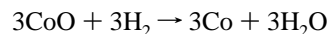
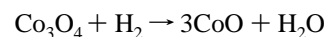


Figure 8. TPR profiles of three bimetallic cobalt/tungsten catalysts. The TPR was conducted with 5% H₂/Ar at a heating rate of 8 °C/min.

In any case, from the reduction profiles it is possible to identify the presence of Co and Mo or Co and W species in the absence of interactions. Accordingly, the TPR of the bimetallic Co:Mo(1:3)/SiO₂ and Co:W(1:3)/SiO₂ catalysts indicates that, in these samples, the vast majority of Co oxide species are interacting either with Mo or W. It is clear that while most of the Co in the monometallic catalyst gets reduced below 500 °C, almost no reduction takes place below this temperature in the bimetallic catalysts. It has been proposed that the addition of Mo oxide to Co oxide inhibits the reduction of the Co species because Mo⁶⁺ polarizes the Co–O bonds, making them more ionic and consequently more difficult to reduce;¹⁵ we can extend this idea to the bimetallic CoW system. In agreement with the DRS and EXAFS/XANES data, TPR indicates that a high degree of Co–W interaction is observed for the catalyst with a low Co:W ratio.

As shown in Figure 8, a gradually increasing fraction of segregated Co species as a function of the Co:W ratio is apparent from the peaks growing at 350 and 450 °C. It has previously been reported that the reduction of Co₃O₄ to Co passes through an intermediate phase (CoO) before the metallic state is reached, following a two-step reduction route that proceeds as¹⁶



Therefore, in the overall process, 1 mol of H₂ is first consumed to produce CoO, and 3 mol of H₂ is consumed to produce the metal. The anticipated ratio of the area of the first peak at 350

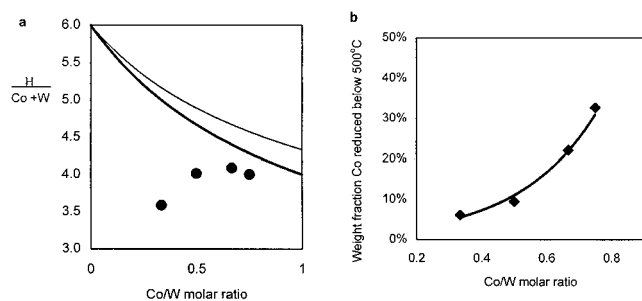


Figure 9. (a) Hydrogen consumption for four CoW/SiO₂ catalysts with different compositions, expressed as the H/[Co + W] molar ratio. Theoretical consumptions for two limiting cases are shown with solid lines. Heavy line: Co and W forming CoWO₄ with the excess W forming WO₃. Light Line: Co and W segregated as Co₃O₄ and WO₃, respectively. (b) Fraction of cobalt reduced to the metallic state after treatment with H₂ at temperatures below 500 °C as a function of Co:W nominal ratio, as determined by calculating the hydrogen uptake from the TPR profiles.

°C with the broader peak at 450 °C should then be close to 0.33, which is in perfect agreement with values obtained for the ratio between the areas of both peaks (0.33 ± 0.02). The peak at 350 °C was, therefore, assigned to the reduction of Co₃O₄ to CoO while the peak at 450 °C peak corresponded to reduction of CoO to Co. The peaks appearing at temperatures above 600 °C should be attributed to reduction of species for which there exists a range of degrees of interaction between the tungsten oxide and Co.

Another interesting trend can be observed in the amount of hydrogen consumed during the TPR process as calculated by integrating the area under the TPR peaks. The total consumption of hydrogen during the TPR process is expressed as H/[Co + W], where H is the molar uptake of atomic hydrogen and Co + W is the total molar content of metal in the sample. The total hydrogen consumptions of the catalysts can be compared to the theoretical consumption that would result in two limiting cases (see Figure 9a). In the first limiting case, Co and W interact forming CoWO₄ and in the second case they are segregated as Co₃O₄ and WO₃, respectively. In the first assumption, all the cobalt would be as CoWO₄ whereas the residual W would be as WO₃. Accordingly, the maximum hydrogen consumption H/[Co + W] for a Co:W ratio of 0 (i.e., only W present as WO₃) would be 6. For a Co:W ratio of 1, the value would be 4 because all the cobalt and tungsten would be as CoWO₄. At an intermediate Co:W ratio, such as 0.5, both CoWO₄ and WO₃ would be present and the hydrogen consumption value would be 4.67. On the other hand, for the other limiting case in which Co and W do not interact and are only forming Co₃O₄ and WO₃, respectively, the hydrogen consumption values for total reduction would range from 6 to 4.88 as the Co:W ratio increases from 0 to 1. A comparison of these limiting cases with the experimental data in Figure 9a indicates that the reduction of Co and W species is not complete because the hydrogen consumption in all catalysts is much lower than the theoretical values for any of the two limiting cases. What is clear is that the reducibility of the catalysts increases with the Co:W ratio. One expects that as the Co:W ratio increases, the fraction of cobalt in the form of noninteracting Co₃O₄ will also increase. However, if only Co₃O₄ gets reduced, the total hydrogen consumption would only be 2.67. Therefore, a partial reduction of the tungsten species also occurs during the TPR. To quantify the fraction of noninteracting Co, we use the area under the first two hydrogen consumption peaks. Figure 9b shows the results of these calculations. Because the cobalt

loading was the same in all the catalysts, the observed trend makes obvious that the amount of cobalt interacting with W increases with the W loading; that is, decreasing Co:W ratio.

3.1.4. Raman Spectroscopy. Figure 10 shows the Raman spectra of the CoMo and CoW catalyst series; the Raman spectrum of an analytical sample of cobalt oxide (Co₃O₄) is also shown. The assignment for the Raman active phonon modes displayed in the spectrum of Co₃O₄ are as follows: the peaks at 199, 621, and 681 cm⁻¹ correspond to F_{2g} phonon modes whereas the peaks at 477 and 525 cm⁻¹ are E_g and A_{1g} phonon modes, respectively.¹⁷ As seen from Figure 10, this set of peaks dominates the spectra of all the bimetallic catalyst with an excess of Co. In agreement with the results obtained by XAS and TPR it is clear that Co₃O₄ is the predominant species of Co present at high Co:W and Co:Mo ratios.

Figure 11 compares the Raman spectrum of the selective bimetallic catalyst, which has a low Co:Mo ratio, with that of reference samples of CoMoO₄ and MoO₃. First, it is clear that segregated Co₃O₄ species are not present on this catalyst, as evidenced by the absence of the characteristic bands described above (199, 621, and 681 cm⁻¹). The peaks appearing in the 750–1000 cm⁻¹ region should be ascribed to Mo species. This is the region where the Raman bands for stretching of Mo–O bonds are expected to appear.¹⁸ Several factors such as metal loading, pH, precursor impregnation method, and impurities are known to influence the exact position of the Raman bands. However, a tentative assignment can be done in light of the results obtained by UV/vis absorption spectroscopy, preceding literature, and the comparison with the reference samples. For instance, the peak centered at 943 cm⁻¹ appearing on the Raman spectrum for the selective Co–Mo (1:3)/SiO₂ catalyst has been previously ascribed to Mo₇O₂₄⁻⁶ species whereas the shoulder at 960 cm⁻¹ has been associated with larger clusters of MoO_x species such as Mo₈O₂₆.^{4,18–20} This assignment agrees with our previous UV/vis spectroscopy results, which suggested the presence of well-dispersed clusters of MoO_x that, according to the calculated band energy gap, corresponded to an average domain size slightly larger than that of Mo₇O₂₄⁻⁶.

According to previously reported results, the presence of large polymeric MoO_x species must be ruled out when there are no peaks in the 990–1000 cm⁻¹ region.^{21,22} Our results further support these conclusions. Indeed, a comparison between the Raman spectra of this catalyst and that of the MoO₃ reference indicates that such species is not present in the catalyst. The relatively high dispersion of Mo oxide might result from the interaction with cobalt,^{14,23–27} i.e., formation of a surface Co molybdate species as previously suggested.⁶ Moreover, the comparison of the Raman spectrum of the bimetallic catalyst with that of the CoMoO₄ shown in Figure 11 gives strong support to the presence of this species. Therefore, the Raman band at 880 cm⁻¹, the shoulder at 930 cm⁻¹, and the broad band at 350 cm⁻¹ must all be assigned to Mo–O–Co stretching vibrations in cobalt molybdate species.^{19,28–31}

3.2. Production of Single-Walled Carbon Nanotubes by Catalytic Disproportionation of CO. As we have reported in previous articles,^{5,6,10} the silica-supported Co–Mo system displays a very high selectivity in the production of single wall nanotubes by CO disproportionation.¹⁰ Interestingly, the high yields and selectivities to SWNT were only obtained after a specific sequence of calcination at 500 °C in air and reduction in H₂ at 500 °C. It is noteworthy to mention that when the Co:Mo(1:3)/SiO₂ catalyst that exhibited a high yield and selectivity toward SWNT was employed without the reduction step or with an exceedingly high reduction temperature, poor SWNT yields

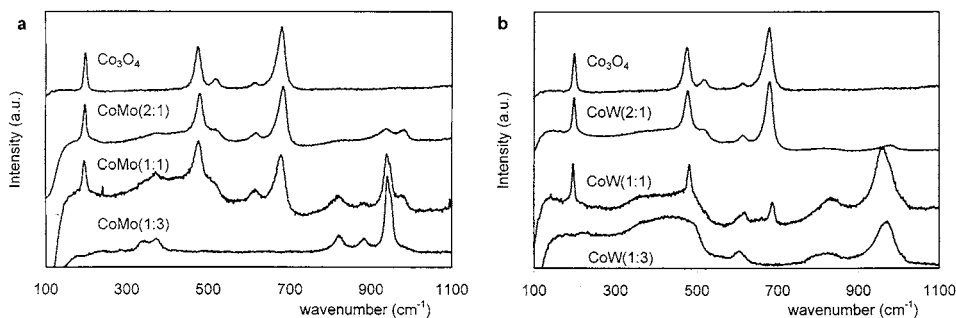


Figure 10. Raman spectra of various supported CoMo/SiO₂ (a) and CoW/SiO₂ (b) catalysts. The spectrum of an analytical sample of cobalt oxide (Co₃O₄) is also shown. The laser excitation energy was 633 nm.

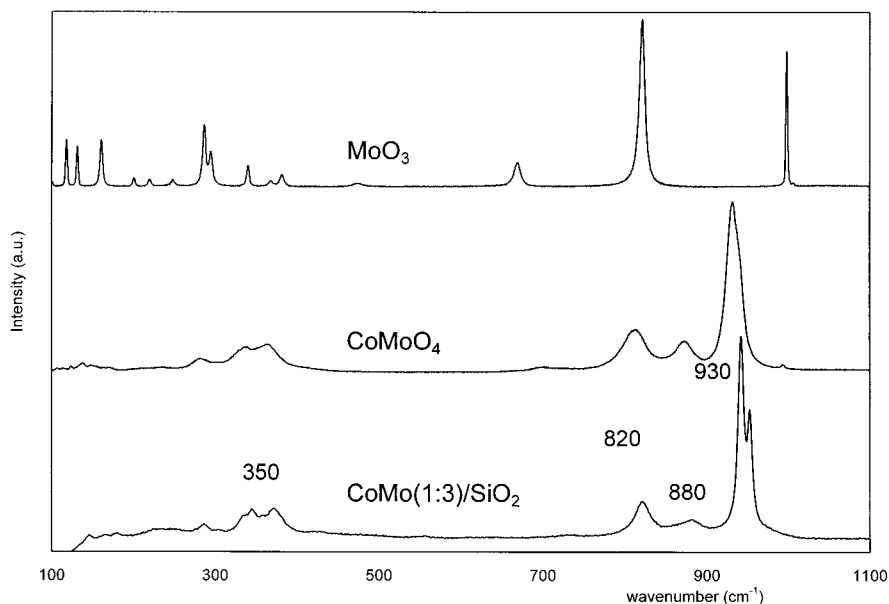


Figure 11. Comparison between the Raman spectra of a selective CoMo (1:3)/SiO₂ catalyst and that of two reference samples of MoO₃ and CoMoO₄. The laser excitation energy was 633 nm.

were attained. We have previously found that with the CoMo catalyst a prereluction step in hydrogen was critical to obtain an active and selective catalyst.⁵ In the present work, we have investigated a CoW(1:3)/SiO₂ catalyst for SWNT production after different prereluction treatments. The reaction temperature for the CO disproportionation after a prereluction step was also varied from 750 up to 950 °C. At the end of a 2-h reaction period, the spent catalyst containing the carbon deposits was cooled in He flow. The characterization of the carbon deposits was done by way of three techniques that we have previously used and tested. They are temperature programmed oxidation (TPO), transmission electron microscopy (TEM), and Raman spectroscopy.

We have shown that from the TPO analysis one can obtain a quantitative measure of the carbon yield and selectivity toward SWNT.⁵ The TPO results obtained in this study are summarized in Table 1 and illustrate the strong influence of the reaction temperature and catalyst pretreatment on SWNT yield and selectivity. In addition to TPO, Raman spectroscopy provides valuable information about the structure of carbon nanotubes. The analysis of the radial A_{1g} breathing mode (below 300 cm⁻¹) gives direct information about the tubes diameter,³² whereas the analysis of the G band in the tangential mode range, i.e., 1400–1700 cm⁻¹, provides information on the electronic properties of the nanotubes. In addition, the analysis of the so-called D band at around 1350 cm⁻¹ gives an indication of the level of disordered carbon. The size of the D band relative to

the G band at around 1590 cm⁻¹ has been used as qualitative measurement of the formation of undesirable forms of carbon.^{33,34} Figure 12 shows the Raman spectra obtained on the carbon deposits formed on the CoW(1:3)/SiO₂ catalyst for different reduction pretreatments. A pronounced variation is observed in the carbon structures produced with the same catalyst after different reduction temperatures. Table 1 shows the parameter (1 – D/G), which we have previously used as a quality indicator for the carbon products obtained using these different reduction treatments. In this parameter D and G are the integrated areas of the D (disorder) and G bands, respectively. A (1 – D/G) parameter approaching unity is representative of a high-quality product. As can be observed in Figure 12 and Table 1, the sample pretreated in H₂ at 900 °C exhibited a high (1 – D/G) quality parameter, whereas the samples pretreated at lower temperatures show much lower values, which indicates the presence of undesirable forms of carbon. As we approach 900 °C, which seems to be the optimal pretreatment temperature, the (1 – D/G) parameter increases; however, when we prerelucted the catalyst at 1000 °C, the selectivity decreased once again. We can attribute this last observation to a high degree of reduction of the catalyst, causing the appearance of large metallic Co, which has been shown to be disadvantageous for SWNT selectivity.⁶ The results previously reported for a highly selective CoMo catalyst are also included in Table 1; it can be observed that although under the right conditions a CoW

TABLE 1: Carbon Yield and Selectivity (Expressed as the D/G Band Area Ratio Obtained from the Raman Spectra) for Carbon Deposits Obtained by CO Disproportionation under Different Pretreatments and Reactions Conditions over CoW(1:3)/SiO₂ and CoMo(1:3)/SiO₂ Catalysts^a

catalyst	reduction temp (°C)	reaction temp (°C)	yield (% C)	1 - D/G quality parameter
CoW(1:3)/SiO ₂	500	850	9	0.20
CoW(1:3)/SiO ₂	600	850	10	0.54
CoW(1:3)/SiO ₂	700	850	6.5	0.68
CoW(1:3)/SiO ₂	800	850	8	0.70
CoW(1:3)/SiO ₂	900	850	9	0.86
CoW(1:3)/SiO ₂	1000	850	6	0.33
CoW(1:3)/SiO ₂	900	750	8	0.54
CoW(1:3)/SiO ₂	900	1000	3	0.88
CoMo(1:3)/SiO ₂	500	850	12	0.95

^a The yield is defined as mass of total deposited carbon per mass of catalyst. the selectivity to SWNT is the mass of SWNT per total mass of carbon deposits.

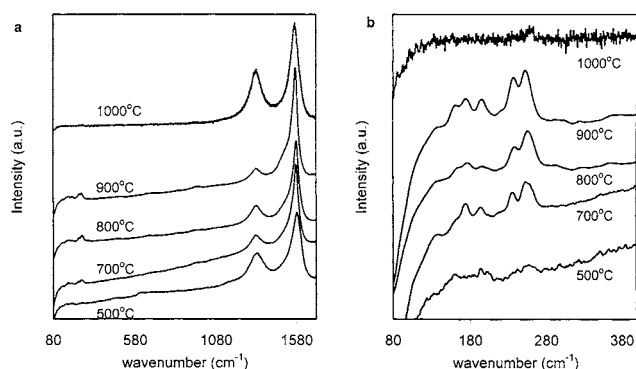


Figure 12. (a) Raman spectra of the carbon deposits obtained by disproportionation of CO at 850 °C over a CoW(1:3)/SiO₂ catalyst after different pretreatment temperatures in hydrogen. (b) Detail of the breathing mode band. The laser excitation energy was 514 nm.

catalyst shows a relatively high selectivity toward SWNT formation, the performance of the selective CoMo catalyst is superior.⁴⁰

Another interesting result is shown in Figures 13 and 14, which depict the Raman spectra obtained for SWNT grown over the CoW(1:3)/SiO₂ catalyst at different reaction temperatures after pretreatment at the optimal reduction temperature of 900 °C. The spectra were taken using two different laser excitation energies to get a more accurate description of the SWNT diameter distribution in our samples. It is known that Raman spectroscopy of SWNT results from a resonant process associated with optical transitions in the one-dimensional electronic density of states, which fall in the visible and near-infrared range^{35,36} and the energy of the allowed optical transitions depends both on the diameter and on the metallic or semiconductor character of the tubes.^{37,38} Consequently, when the excitation energy is close to that of an allowed optical transition for a specific type of nanotube, the Raman intensity is greatly enhanced. Therefore, when different excitation energies are employed, different nanotubes can be probed. Figures 13 and 14 also include the radial breathing mode (RBM) region for three different SWNT samples, obtained with two different laser excitation energies. Although for a given sample the spectra are quite different depending on the laser excitation energy used, the same trend is observed at both energies; that is, the RBM bands shift to lower frequencies as the reaction temperature increases. Because the frequency of the radial breathing mode is inversely proportional to the nanotube diameter,³³ this shift indicates that, as we previously reported for the CoMo system,

the average nanotube diameter increases when higher reaction temperatures are used.^{39,40}

4. Discussion

In previous communications we have reported the characterization results obtained on the Co:Mo system during the production of SWNT.⁶ The most important results of previous studies were that the extent of the Co–Mo interaction was a function of the Co:Mo ratio in the catalyst and that this interaction had different forms during the different stages of the catalyst life. For example, we found that in the calcined state, Mo was in the form of a well-dispersed Mo(VI) oxide whereas the state of Co strongly depended on the Co:Mo ratio. At low Co:Mo ratios, it interacted with Mo forming a superficial Co molybdate-like structure. At high Co:Mo ratios, it forms a noninteracting Co₃O₄ phase. During the subsequent reduction treatment in hydrogen, the noninteracting Co phase reduced to metallic Co, whereas the Co molybdate-like species remained as well-dispersed Co²⁺ ions.

We showed that the effect of having Co stabilized in the Co–molybdate environment was crucial. First of all, this stabilization prevented the sintering of Co into large metallic aggregates, which generates undesired forms of carbon, as it occurs in the nonselective catalysts. By contrast, when metal atoms begin to agglomerate on the selective catalyst in the presence of gaseous CO, there was a nucleation period over which there was no growth of nanotubes. This nucleation involved the disruption of Co atoms from its interaction with Mo oxide when the latter became carbidic.

In the characterization of the CoW catalyst series reported in this work, we have found a strong similarity and some interesting differences with the CoMo system described above. The UV/vis and the X-ray absorption data indicate that similar to the case of Mo, in the calcined catalyst, W is in an octahedral environment and in the VI oxidation state. Furthermore, from the values of the adsorption edge energy it can be concluded that the tungsten oxide species are forming small clusters with average domain sizes to some extent larger than those of the metatungstate ion, but not large enough to form bulk WO₃. The majority of W seems to be forming these oxidic species, regardless of the Co:W ratio in the catalysts; although for catalysts with higher W loadings (i.e., CoW(3:4)/SiO₂), contribution of larger WO_x species becomes apparent (see Figure 1). Therefore, it appears that the W dispersion is more a result of the metal loading and the degree of interaction with the support rather than a consequence of the extent of interaction with Co. A contrasting picture is obtained from the Co side, particularly in the catalysts with low Co:W ratio. In this case, both the UV/vis and XANES data of the catalyst with a Co:W ratio of 1:3 demonstrated that most of the Co is in an environment similar to that in CoWO₄ i.e., closely interacting with W. However, the slight but clear differences between the spectra of the catalyst and the CoWO₄ reference suggest that the similarity is limited to the local environment and nature of ligands. In fact, the EXAFS data demonstrate that bulk CoWO₄ is not present in the bimetallic catalysts.

The results for the calcined catalysts with low Co:W ratios can be put together in a simple model. Similar to our description of the Co–Mo system, we propose that in the Co–W catalysts dispersed Co species get stabilized over the tungsten oxide in the form of a CoWO₄-like layer. This layer is thin enough, so although most of the Co is in this Co–W interacting phase, only a small fraction of W forms part of such a phase, and the rest remains as tungsten oxide. Therefore, the characterization

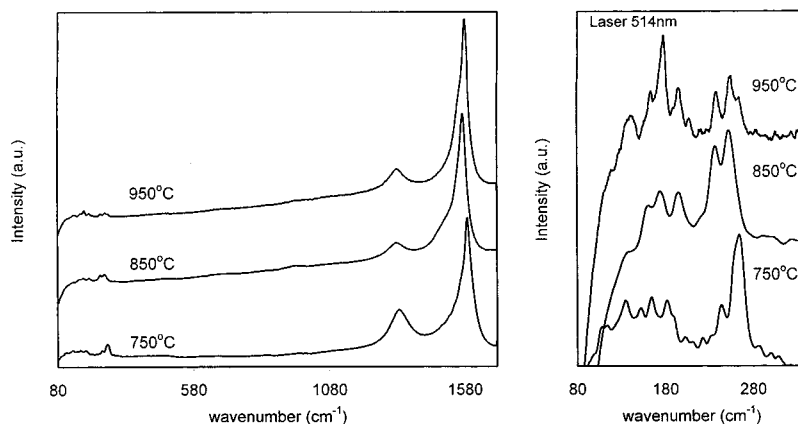


Figure 13. Raman spectra of the SWNT growth by disproportionation of CO at 750, 850, and 950 °C over a CoW(1:3)/SiO₂ catalyst after a pretreatment at 900 °C in hydrogen. Right: Detail of the breathing mode band. The laser excitation energy was 514 nm.

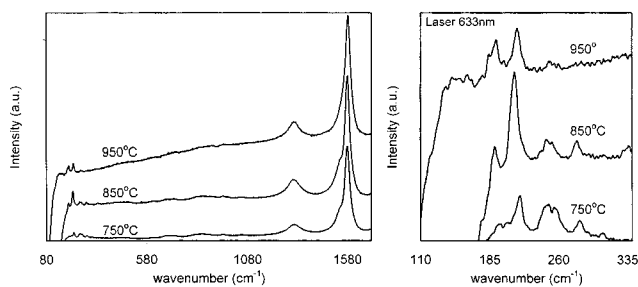


Figure 14. Raman spectra of the SWNT growth by disproportionation of CO at 750, 850, and 950 °C over a CoW(1:3)/SiO₂ catalyst after a pretreatment at 900 °C in hydrogen. Right: Detail of the breathing mode band. The laser excitation energy was 633 nm.

of W does not reflect a strong interaction with Co, whereas the characterization of Co shows, in fact, a high degree of interaction with W. In this context, we need to stress that it is necessary to have an excess of W to guarantee the formation of this cobalt tungstate phase. Otherwise, more than one type of Co species will be present and the catalyst becomes unselective. For example, the UV/vis–DRS data clearly show that in addition to the interacting phase of Co, which dominates at low Co:W ratios, a noninteracting phase begins to form as the W content decreases. The X-ray absorption data (Figure 5) together with the results obtained from the TPR and Raman experiments undoubtedly show that this noninteracting species is Co₃O₄.

In previous work,^{5,6} we have proposed that the role of Co is the activation of CO, whereas the role of Mo is the stabilization of Co(II) ions. When Co is not interacting with Mo, in the reduced state it sinters and forms large metal aggregates. These large metallic Co aggregates have the tendency to generate defective MWNT, carbon filaments, and graphite nanofibers. However, when Mo is present in the catalyst and there is no excess of free Co, a well-dispersed Co²⁺ species in the form of a Co molybdate-like phase is stabilized. From the detailed studies conducted over the CoW system reported in this contribution, we can propose that the formation of a similar interacting Co tungstate-like species plays a determinant role in the catalytic activity toward the formation of SWNT.

Equally important, we found that in the case of the Co–Mo system a prereluction step at 500 °C in hydrogen before starting the nanotube growth was essential to maximize the SWNT selectivity. As we have previously proposed, certain degree of reduction associated with the creation of oxygen vacancies around Mo (or W) is necessary because a catalyst fully oxidized before the reaction is not efficient.⁶ By contrast, a high degree of reduction before the reaction is detrimental for the selectivity

toward SWNT.⁵ It is suggestive that the TPR profile shown above for the CoMo(1:3) sample indicates that reduction of the Co–Mo pair does not start until about 500 °C, whereas the corresponding result for the CoW system shows that for this case the reduction begins at 750 °C. In agreement with the previous behavior observed for the Co–Mo catalyst, a poor performance of the CoW catalysts is observed when it is pretreated at a temperature lower than the onset of reducibility, in this case about 750 °C. The data in Table 1 and the Raman spectra in Figure 12 show that very low selectivities are achieved with low reduction temperatures. The optimum prereluction treatment is around 900 °C.

The Raman spectra of the carbon deposits obtained over the selective catalyst at different reaction temperatures are consistent with those previously observed for the Co–Mo system. That is, as the reaction temperature increases, the diameter of the tubes increases.^{39,40} We postulate that in both cases (Co–Mo and Co–W systems) Co atoms agglomerate in the presence of gaseous CO within a nucleation period over which there is no growth of nanotubes. This in-situ nucleation involves the disruption of Co atoms from its interaction with Mo or W oxide. This disruption is followed by surface migration leading to agglomeration into mobile clusters that continue to grow under the bombardment of CO molecules. Some of these molecules decompose and carbon in the Co cluster begins to rearrange (nucleate) until a given configuration and carbon concentration are reached, which favor the phase segregation and formation of a hemispherical shell over the particle, which finally will break its symmetry and lead to SWNT formation.⁴¹ We have called this configuration *embryo*.⁴² When this embryo is formed, the subsequent incorporation of carbon and SWNT growth proceeds at a fast rate, perhaps only controlled by mass transfer. Because the sintering of Co clusters accelerates with temperature, a higher density of larger metal clusters can be expected on the catalyst surface as temperature is increased. These larger clusters are in turn responsible for the formation of larger embryos, and in turn, tubes of larger diameter.

5. Conclusions

We can summarize the main findings of the present work in the following conclusions:

(a) As in the case of the Co–Mo system, the selectivity of the Co–W catalysts toward SWNT production by CO disproportionation strongly depends on the stabilization of Co²⁺ species, which results from an interaction with W. The extent of this interaction is inversely proportional to the Co:W molar ratio. At high Co:W ratios, there exists a fraction of Co not

stabilized by W and that fraction is responsible for a decrease in selectivity.

(b) In the oxidic state after calcination, W is forming small clusters in the form of well-dispersed W (VI) species and Co is either interacting with W in a superficial Co tungstate-like structure (at low Co:W ratios) or not interacting, forming a Co₃O₄ phase (at high Co:W ratios).

(c) During the subsequent reduction treatment, the noninteracting phase is reduced to metallic Co, whereas the Co tungstate-like species remain as well-dispersed Co²⁺ ions.

(d) The reduction treatment is critical for the good performance of the selective Co–W catalyst, the highest selectivity is reached when the catalyst is prereduced at 900 °C; higher reduction temperatures create large metallic Co particles which are responsible for selectivity losses.

(e) The sintering of the Co clusters, which accelerates with temperature, controls the diameter of the growing SWNT. By running the reaction at higher temperatures, tubes of larger diameters are obtained.

Acknowledgment. This research was conducted with financial support from the Department of Energy, Office of Basic Energy Sciences (grant No. DE-FG03-02ER15345). Technical support from the personnel at NSLS, Brookhaven National Lab, for the EXAFS experiments is gratefully acknowledged. J.E.H. thanks the Fulbright-CAREC program for a scholarship.

References and Notes

- (1) Yakobson, B. I.; Smalley, R. E. *Am. Sci.* **1997**, 85, 324.
- (2) Kong, J. A.; Cassell, A. M.; Dai, H. *Chem. Phys. Lett.* **1998**, 292, 567.
- (3) Nikolaev, P.; Bronikowski, M. J.; Bradley R. K.; Rohmund, F.; Colbert, D. T.; Smith, K. A.; Smalley, R. E. *Chem. Phys. Lett.* **1999**, 313, 91.
- (4) Dai, H. *Surf. Sci.* **2002**, 500, 218.
- (5) Kitiyanan, B.; Alvarez, W. E.; Harwell, J. H.; Resasco, D. E. *Chem. Phys. Lett.* **2000**, 317, 497.
- (6) Herrera, J. E.; Balzano, L.; Borgna, A.; Alvarez, W. E.; Resasco, D. E. *J. Catal.* **2001**, 204, 129.
- (7) Topsøe, H.; Clausen, B. S.; Massoth, F. E. *Hydrotreating Catalysis*; Springer-Verlag: Berlin, 1996.
- (8) Kishan, G.; Coulier, L.; van Veen, J. A. R.; Niemantsverdriet, J. W. *J. Catal.* **2001**, 200, 194.
- (9) Coulier, L.; Kishan, G.; van Veen, J. A. R.; Niemantsverdriet, J. W. *J. Phys. Chem. B* **2002**, 106, 5897.
- (10) Alvarez, W. E.; Kitiyanan, B.; Borgna, A.; Resasco, D. E. *Carbon* **2001**, 39, 547.
- (11) Barnton, D. G.; Shtein, M.; Wilson, R. D.; Soled, S. L.; Iglesia, E. *J. Phys. Chem. B* **1999**, 103, 630.
- (12) Weber, R. S. *J. Catal.* **1995**, 151, 470.
- (13) Kasper, H. *Monatsh. Chem.* **1967**, 98, 2104.
- (14) Gajardo, P.; Grange, P.; Delmon, B. *J. Phys. Chem.* **1979**, 83, 1771.
- (15) Halawy, S.; Mohamed, M.; Bond, G. *J. Chem. Technol. Biotechnol.* **1993**, 58, 237.
- (16) Li, J.; Jacobs, G.; Zhang, Y.; Das, T.; Davis, B. H. *Appl. Catal. A Gen.* **2002**, 223, 195.
- (17) Hadjiev, V. G.; Iliev, M. N.; Vergilov, I. V. *J. Phys. C: Solid State Phys.* **1988**, 21, L199.
- (18) Mestl, G.; Srinivasan, T. K. *Chem. Rev. Sci. Eng.* **1998**, 40, 451.
- (19) Brown, F. R.; Makovsky, L. E.; Rhee, K. H. *J. Catal.* **1977**, 50, 162.
- (20) La Parola, V.; Deganello, G.; Tewell, C. R.; Venezia, A. M. *Appl. Catal. A Gen.* **2002**, 235, 171.
- (21) Williams, C. C.; Ekerdt, J. G.; Jehng, J. M.; Hardcastle, F. D.; Turek, A. M.; Wachs, I. E. *J. Phys. Chem.* **1991**, 95, 8781.
- (22) Radhakrishnan, R.; Reed, C.; Oyama, S. T.; Seman, M.; Kondo, J. N.; Domen, K.; Ohminami, Y.; Asakura, K. *J. Phys. Chem. B* **2001**, 105, 8519.
- (23) Topsøe, N. Y.; Topsøe, H. *J. Bull. Chim. Belg.* **1981**, 90, 1311.
- (24) Topsøe, H.; Clausen, B. S.; Candia, R.; Wivel, C.; Mørup, S. *Bull. Soc. Chim. Belg.* **1981**, 12, 1187.
- (25) Topsøe, H.; Clausen, B. S.; Burriesci, N.; Candia, R.; Mørup, S. In *Preparation of Catalysts II*; Delmon, B., Grange, P., Jacobs, P. A., Poncelet, G., Eds.; Elsevier: Amsterdam, 1979; p 479.
- (26) de Boer, M.; Koch, E. P. F. M.; Blaauw, R. J.; Stobbe, E. R.; Hoffmann, A. N. J. M.; Boot, L. A.; van Dillen, A. J.; Geus, J. W. *Solid State Ionics* **1993**, 63, 736.
- (27) Gajardo, P.; Pirotte, D.; Grange, P.; Delmon, B. *J. Phys. Chem.* **1979**, 83, 1780.
- (28) Li, Z.; Fu, Y.; Bao, J.; Jiang, M.; Hu, T.; Liu, T.; Xie, Y.-N. *Appl. Catal. A: Gen.* **2001**, 220, 21.
- (29) Clark, G. M.; Doyle, W. P. *Spectrochim. Acta* **1966**, 22, 1441.
- (30) Trifiro, F.; Centola, P.; Pasquon, I. *J. Catal.* **1968**, 10, 86.
- (31) Kuang, W.; Fan, Y.; Chen, K.; Chen, Y. *J. Catal.* **1999**, 186, 310.
- (32) Rao, A. M.; Richter, E.; Bandow, S.; Chase, B.; Eklund, P. C.; Williams, K. A.; Fang, S.; Subbaswamy, K.; Menon, M.; Thess, A.; Smalley, R. E.; Dresselhaus, G.; Dresselhaus, M. S. *Science* **1997**, 275, 187.
- (33) Rols, S.; Righi, A.; Alvarez, L.; Anglaret, E.; Almairac, R.; Journet, C.; Bernier, P.; Sauvajol, J. L.; Benito, A. M.; Maser, W. K.; Munoz, E.; Martinez, M. T.; de la Fuente, G. F.; Girard, A.; Ameline, J. C. *Eur. Phys. J. B* **2000**, 18, 201.
- (34) Bandow, S.; Asaka, S.; Saito, Y.; Rao, A. M.; Grigorian, L.; Richter, E.; Eklund, P. C. *Phys. Rev. Lett.* **1998**, 80, 3779.
- (35) Pimenta, M. A.; Marucci, A.; Empedocles, S. A.; Bawendi, M. G.; Hanlon, E. B.; Rao, A. M.; Eklund, P. C.; Smalley, R. E.; Dresselhaus G.; Dresselhaus, M. S. *Phys. Rev. B* **1998**, 58, R16016.
- (36) Richter, E.; Subbaswamy, K. R. *Phys. Rev. Lett.* **1997**, 79, 2738.
- (37) Kataura, H.; Kumazawa, Y.; Maniwa, Y.; Umez, I.; Suzuki, S.; Ohtsuka Y.; Achiba, Y.; *Synth. Met.* **1999**, 103, 2555.
- (38) Corio, P.; Brown, S. D. M.; Marucci, A.; Pimenta, M. A.; Kneipp, K.; Dresselhaus, G.; Dresselhaus, M. S. *Phys. Rev. B* **2000**, 61, 13202.
- (39) Alvarez, W. E.; Pompeo, F.; Herrera, J. E.; Balzano, L.; Resasco, D. E. *Chem. Mater.* **2002**, 14, 1853.
- (40) Herrera, J. E.; Balzano, L.; Pompeo, F.; Resasco, D. E. *J. Nanosci. Nanotechnol.*, in press.
- (41) Melechko, A. V.; Merkulov, V. I.; Lowndes, D. H.; Guillorn, M. A.; Simpson, M. L. *Chem. Phys. Lett.* **2002**, 356, 527.
- (42) Resasco, D. E.; Alvarez, W. E.; Pompeo, F.; Balzano, L.; Herrera, J. E.; Kitiyanan, B.; Borgna, A. *J. Nanoparticle Res.* **2002**, 4, 131.